

Role of alloy spacer layers in non top-on-top vertical correlation in multistacked systems

Catherine Priester

IEMN, Département ISEN, CNRS-UMR 8520, BP 69 F-59652 Villeneuve d'Ascq, Cedex, France

Geneviève Grenet

Ecole Centrale de Lyon, LEOM, CNRS-UMR 5512, BP 163 F-69131 Ecully Cedex, France

(Received 18 April 2001; published 10 September 2001)

We focus on the role of spacer alloy decomposition in the vertical correlation for a bilayer of strained InAs quantum wires, where the spacer layer is an immiscible alloy. We show how the surface morphology combined with the strongly inhomogeneous strain distribution favors a V-shaped partial demixing of the spacer layer. We also demonstrate that this decomposition has tangible consequences on the vertical organization when depositing a second wire layer. Different configurations can be obtained from perfect top-on-top, to perfect vertical anticorrelation, via all kinds of oblique correlation.

DOI: 10.1103/PhysRevB.64.125312

PACS number(s): 68.65.-k, 61.66.Dk, 64.75.+g, 81.40.Jj

I. INTRODUCTION

It is presently well accepted that, when growing multilayer arrays of coherently strained islands, the strain distribution due to the layer of buried dots favors the vertical alignment organization.¹⁻³ For systems grown on (100) substrates, experiments⁴⁻⁸ have mainly shown vertical alignment between two successive dot layers. In a recent letter, Holý *et al.*⁹ claimed that all forms of vertical and lateral correlation can be explained by taking into account the elastic anisotropy of the matrix material with respect to the growth orientation. They showed that in the case of stacked dot layers (viewed as buried point stress source layers), the usual vertical correlation could be affected by a strong matrix elastic anisotropy leading to a nonvertical dot stacking. They have used this approach to explain the fcc-like stacking organization of PbSe dots in a $\text{Pb}_{1-x}\text{Eu}_x\text{Te}$ (111) matrix.¹⁰ Similar arguments (invoking anisotropy) have been used by Shchukin *et al.*¹¹ for CdSe/ZnSe. However, in the case of (001) substrates and III-V semiconductors with an anisotropic parameter $A = 2C_{44}/(C_{11}-C_{12})$ close to 2, the depth of the minima (compared to the vertical position energy) is very weak, and, if the spacer layer is not too thick, the minima are located so close to the perfect vertical of the buried dots, that vertical stacking is still expected.

On the other hand, in the case where the spacer layers are immiscible alloys, partial alloy decomposition may act against the classically observed top-on-top vertical dot organization and lead to a new vertical dot organization. Such an effect has been recently reported for InAs wires in InAlAs alloy lattice-matched on InP(001) (Ref. 12) and referred to as a staggered type vertical organization. Nothing similar has been found for InP as spacer layer material, the vertical dot organization still being of the top-on-top type.¹³ Furthermore, we have already shown¹⁴ that strains and non flat surface morphology can combine in order to favor significant alloy demixing. In the next section of this paper, we will extend this theoretical study to the case of InAs quantum wires deposited on a substrate lattice-matched to InP, and calculate which distribution of alloy decomposition is liable

to occur during the burying process. Section III will be devoted to the study of how such partial spacer alloy decomposition will modify the optimal nucleation location of the upper wire layer. Depending on their size and on the spacer layer thickness, the upper wires will be shown to be located either in perfect vertical correlation or in total or partial vertical anticorrelation with respect to the first wire layer positions.

II. STRAIN-INDUCED SPACER ALLOY DECOMPOSITION DURING THE BURYING PROCESS

On one hand, we have previously shown¹⁴ that, when an immiscible alloy is deposited layer-by-layer on a rough surface, alloy demixing appears to be an efficient way to partly relax the strains in the system (and this is true for both lattice-matched and mismatched alloys). That is to say that a rough morphology can allow the relaxation of intrinsic strain energy (i.e., the mixing enthalpy) as well as extrinsic strain energy (i.e., from a lattice mismatch with the substrate).

On the other hand, the strained deposited InAs quantum wires provide a clearly nonhomogeneous surface strain distribution that also can allow partial alloy decomposition. Consequently, when burying a 3D strained wire in an alloy, both these phenomena (strong deviation from flat surface plus non-homogeneous surface strain) have to be taken into account. Using the formalism previously described in Ref. 14, based on an atomistic description and making use of Keating's potential, we have calculated the composition distribution in the spacer layer resulting from such a burying of strained wires.

Let us recall here the main characteristics of this formalism. Starting from a fixed morphology (including the buffer layer and the wires), it mimics the layer-by-layer growth of the spacer in such a way that it flattens the surface by filling up spaces between wires. This actually means that we have chosen (i) not to describe "exactly" the modification of the wire shape during the burying (mainly because it is not as precisely known), but our starting surface morphology is chosen such that the actual theoretical shape of wires

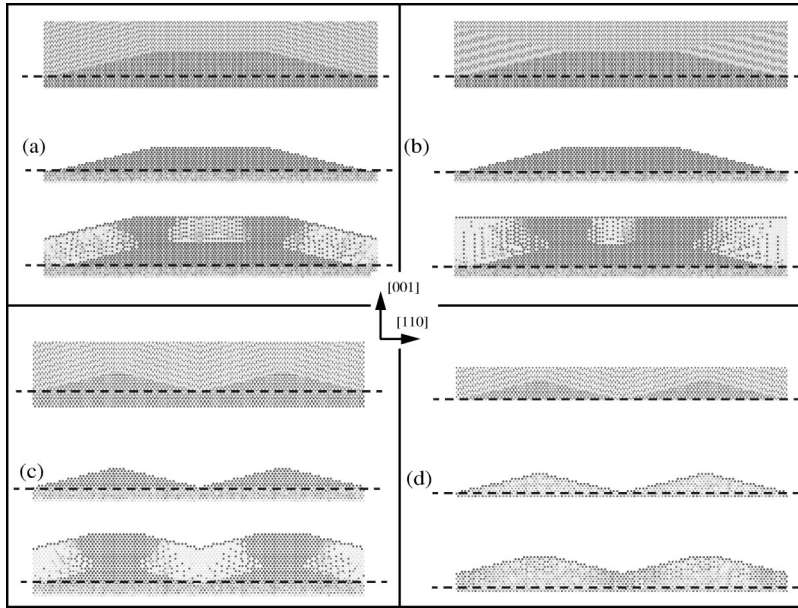


FIG. 1. Cross section views of the alloy distribution resulting from a monolayer-by-monolayer burying of (311) faceted wires. (a) and (b) 40 nm wide, 3.5 nm high InAs wire; (c) 20 nm wide, 2.1 nm high InAs wire, (d) same as (c) but for an InAlAs wire. The different step-by-step growth processes are given in the upper part. The starting morphology is given in the middle part of the figure, and the resulting alloy distribution at the bottom. For more details see text.

matches the experimental one as observed by TEM after burying, (ii) to include (and perhaps to emphasize a bit) the smoothing of the growth front when depositing the lattice-matched spacer layer (such smoothing occurs in order to decrease the surface energy).

It provides the alloy decomposition one would get for very low growth rates, when there is no kinetic limitation that prevents the surface atoms from reaching the optimal distribution that minimizes the total elastic plus surface energy. In other words, kinetic growth conditions far from thermodynamical equilibrium would tend to increase the composition homogeneity of the spacer layer.

It describes *surface* alloy decomposition that occurs *at the growth front* which is quite different from *bulk* spinodal decomposition.

The result is obviously strongly dependent on the way the growth has been described “step-by-step,” as the surface morphology evolution during growth is *not* calculated but simply added to the calculation.

However, because the main aim of this work is to show how spacer alloy decomposition can induce a non-top-on-top vertical dot organization, the actual design of the initial dot geometry as well as the details of the ensuing smoothing are not really of prime importance. Nevertheless, several typical cases will be presented below.

We have represented in Fig. 1 cross sections containing one or two wires for the purpose of clarity (depending on the size of the wire). The alloy decomposition is schematized by making use of grey scale: a dark point represents a pure In atomic row, a bright one a pure Al atomic row and intermediate grey levels are related to the average composition of the corresponding atomic row. The anion rows are withdrawn. The upper diagram shows the details of the step-by-step growth (atoms deposited during successive steps are alternately dark and bright). The starting morphology is given in the middle diagram, and the resulting alloy distribution can be seen at the bottom. The dashed line corresponds to the upper limit of the substrate on which the InAs wires have

been grown. We have considered periodic systems, with two wires per period. Figure 1(a) displays the alloy distribution resulting from a monolayer-by-monolayer burying of InAs wires, 40 nm wide, 3.5 nm high and (113) faceted. A clear In enrichment starting from the upper edges of InAs wires can be observed. This phenomenon is very similar to that observed by transmission electronic microscopy (TEM) experiments in Ref. 12, and that has been called ‘V-shaped arms’. A similar typical alloy composition distribution is obtained if growth is faster on the (113) facets than on the flat (001) areas as in Fig 1(b). This is not the case if the tops of the InAs wires are too narrow, as can be seen in Fig 1(c): the In-rich arms meet and In-rich areas can be found at the vertical of the center of the wires. Last, if the alloy is deposited on artificial InAlAs wires [with the same morphology as in Fig. 1(c), but with no mismatch, thus no strain pattern] as in Fig. 1(d), the alloy demixing is weaker, and In rich areas are located in the valleys between the wires.

These results can be interpreted as follows: demixing in an alloy lattice matched to a substrate is governed by the mixing enthalpy and is possible only because the surface is not perfectly flat. When an InAlAs spacer layer is grown on InAs wires, the most attractive zones for newly deposited In adatoms correspond to In-rich zones, especially those with edges and the farthest possible from the substrate in order to permit the best strain relaxation, viz., the upper edges of the wire in our case. Whether the zone on a wire is completely In rich or not mainly depends on the amount of In deposited during the current step as compared to the number of available sites around the upper edges of the wire. Therefore for either narrow wires or two wires separated by a very large area, the whole upper surface will be In rich, whereas for wide-flat-top wires very close to each other only the upper edges will be In rich, leading to the V-shaped arms. The orientation of the arms depends less on the trajectories of edges during the burying process than on the global surface morphology. The case of Fig. 1(d) is completely different because the initial islands are lattice-matched with a random

atom distribution and thus do not present any initial strain inhomogeneity via In-rich area. Therefore, surface considerations prevail yielding to the usual In surface segregation on sloped areas.¹⁴ When growth is subsequently performed, In atoms concentrate in the valleys between the wires, i.e., the meeting point of two slopes because of the chosen morphology flattening process.

The alloy composition distributions we obtain present almost pure InAs areas. This is simply due to the fact that our description is too deterministic, in the sense that no kinetic limitation is included, and an infinitely slow growth rate is assumed. For simulating a more realistic situation where not all atoms are allowed to reach the more stable configuration, we can arbitrarily add a bit of randomness in the calculation. In this case, the resulting decomposition becomes obviously smoother.¹⁵

In summary, this study shows that when InAs wires are buried in an immiscible alloy, the alloy tends to demix. In-rich arms arising from the top rims of the wires are always present. The actual shape of those arms depends more on the starting morphology than on the deposition process. For wide top wires there are “open” V-shaped arms, whereas for narrow tops there are filled V-shaped In-rich areas. Moreover we have demonstrated in Fig. 1(d) that these V-shaped arms cannot be attributed to purely morphological reasons. Both morphological and strain considerations have to be invoked to explain the actual alloy demixing in buried layers.

III. SPACER ALLOY DECOMPOSITION-INDUCED VERTICAL CORRELATION

The second point to be considered is the way this new composition distribution can modify the optimal nucleation location of the upper wire layer. Here again, we have used a theoretical scheme which has recently been proved to satisfactorily describe the top-on-top multistacked self-organization of Ge islands in an Si matrix.¹⁶ We calculate (within continuous elasticity and making use of the finite differences method) the strain distribution using a given composition pattern. This pattern includes the actual InAs wires buried in an InAlAs layer that presents In-rich V-shaped arms. The main reason for not using in this section the same Keating’s formalism as in the previous section is to free us from too deterministic a growth model which would be inadequate for nucleation calculation (as discussed in Sec. II) which would provide too strong a decomposition in the spacer, capable of altering the resulting nucleation process. Using the actual spacer decomposition appears more helpful.

In this continuous approach alloys are virtual and characterized by their lattice and elastic constants given by Vegard’s law. This description includes the material anisotropy. For the sake of simplicity we have chosen to use a 2D description here. The InAlAs composition is designed continuously in such a way as to provide InAs-rich V-shaped arms. Indium composition decreases with the distance from those V’s, and also with the distance from the edges of the buried wire. The average composition all over the alloy is adjusted to the “lattice-matched to InP composition” (i.e., 0.48 Al concentration). A schematic InAlAs composition distribution

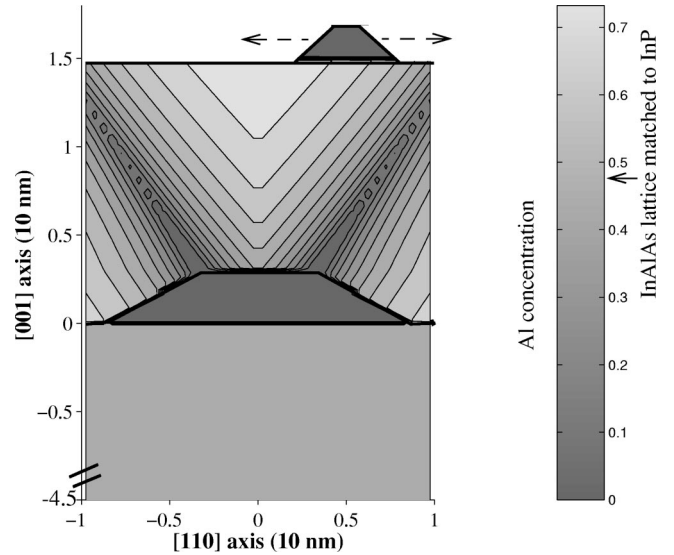


FIG. 2. Composition distribution (in cross-section view) in the system made of a demixed spacer layer, with a surface wire (allowed to move all along the surface) dark corresponds to InAs, medium grey to InAlAs lattice matched to InP, and bright to Al rich InAlAs.

is displayed in Fig. 2. The calculus has been done for geometrical parameters extracted from TEM measurements¹² but for visual requirements, the relative dimensions have been slightly modified in Fig. 2.

When the second InAs layer is deposited, the surface presents some strongly nonhomogeneous strain distribution which is known to favor preferential sites for a new wire nucleation.^{1,2} However, as emphasized in Ref. 16, the surface strain distribution that comes from the buried wire layer is not sufficient to create so-called nucleation sites for *isolated atoms or small clusters*, but is very efficient for organizing large enough 2D or 3D wires on the surface (for adequate spacer layer thicknesses). This efficiency is activated by the elastic interaction between the deposited wires and the buried ones. For this reason we have chosen not only to calculate the surface strain distribution before the deposition of the second wire layer, but to study the variations of the total elastic energy (for buried wires + demixed spacer layer + surface wires) as the surface wire moves all along the surface. Several surface wire widths (i.e., 3.5 to 14 nm) and 2 nm height have been used as elastic interaction probes with buried wire of 17 nm basis width and 3 nm height using a 20 nm period. As observed in TEM measurement the angles between the In-rich arms and the (100) surface is taken as 56° . In Figs. 3(a)–3(c), we have reported the reduced energy variations versus the wire location, for different wire bases (from 3.5 to 14 nm), and varying the spacer thickness from 5 nm (a) to 15 nm (c). “Reduced energy” means the difference between energies with and without surface wires, thus normalized to the corresponding energy of a 2D InAs layer biaxially strained to InP. The period of the system which corresponds to the distance between two buried wires is fixed at 20 nm. Distances are in units of the period, so that 0 corresponds to the perfect vertical anticorrelation (AC), whereas 0.5 corresponds to the perfect vertical correlation

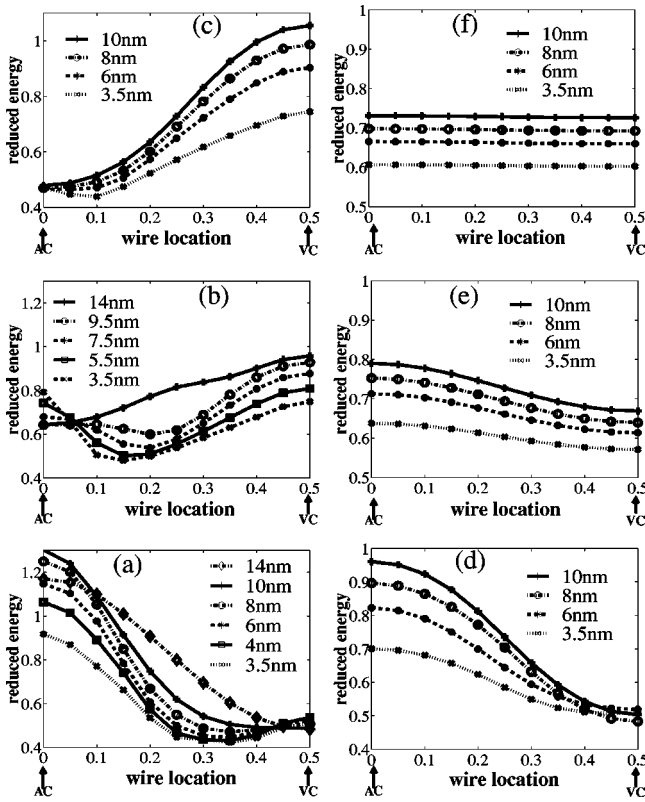


FIG. 3. Reduced energy variations versus the wire location, for different wire bases (from 3.5 to 14 nm), and varying the spacer thickness: 5 nm (a), (d), 10 nm (b), (e), and to 15 nm (c), (f). Distance between two buried wires is fixed at 20 nm. Distances are in units of the period (i.e., the distance between two buried wires fixed at 20 nm). Arrows indicate the perfect vertical anticorrelation (AC) and the perfect vertical correlation (VC). (a)–(c) correspond to a demixed InAlAs spacer layer and (d)–(f) to a uniform concentration in the InAlAs spacer layer.

(VC). To enhance the role of the spacer layer decomposition, we have calculated the same systems, imposing a uniform concentration in the InAlAs spacer layer. These results are given in Figs. 3(d)–3(f).

Let us first consider the case of a very thin spacer layer [Figs. 3(a) and 3(d)]. When any alloy decomposition is forbidden, the well known top-on-top alignment is found. This is not the case for the demixed spacer layer. Here the situation is more complex as the optimal wire location depends on the wire size. For very small wires the optimal wire location is shifted from vertical, leading to an oblique alignment. This corresponds to the crossover between the In-rich arm and the surface. When the wire widens one tends to recover the vertical alignment, which is obtained only for very wide wires (more than half of the period, so that the wire covers the two arms emerging from a given buried wire). Conversely, for a rather thick spacer layer (15 nm), so thick that for a uniform spacer layer (f) there is no longer any driving force for vertical correlation, in the case of demixed spacer layer (c), the optimal location passes from oblique for very small wires to perfect anticorrelation for wider wires. This time anticorrelation corresponds to a wire which covers two

arms merging from two adjacent buried wires. The intermediate situation for a uniform spacer layer (e) is simply between (d) and (f). The case of (b) looks more complicated. This can be viewed as a contest between the oblique minimum observed in (a) and the anticorrelated minimum observed in (c). For small wires the winner is the oblique correlation, whereas for wide wires the winner is the perfect anticorrelation. Let us note that, in the case of oblique correlation, the optimal location shifts towards vertical alignment as the wire widens. The 9.5 nm width corresponds to the switch point.

It is interesting to have a look at the efficiency of the phenomenon. The depth of the minima lies in the same range for Fig. 3(c) (15 nm, demixed) and Fig. 3(d) (5 nm, uniform). This means that alloy decomposition effects, for a wide spacer layer, are as efficient as those of wires buried with a thin spacer without alloy decomposition. This effect definitely does not simply result from the surface composition but from the composition distribution all over the spacer since in the case of Fig. 3(c) the surface composition variations are weak. Here we have not considered kinetic limitations, but simply searched the optimal locations for the surface wires. As a matter of fact kinetic limitations do not appear to be too prohibitive in the present case: if the optimal location moves when the wires widen, finding the optimal location never requires an in-one-go moving of the wire, but simply an asymmetric ripening.

To summarize this study, let us say that compositional effects in the spacer layer appear to be very efficient for organizing surface wires either in oblique correlation or in perfect anticorrelation with the buried wires, depending both on the spacer thickness and on the surface wire size. Note that from a practical point of view, such spacer demixing could affect the electronic properties of the heterostructure by worsening the electronic barrier homogeneity.

IV. CONCLUDING REMARKS

If the concept of multistacked strained deposited layers is actually well known as an attractive way for obtaining nanostructures with a high quality organization the use of immiscible alloy as spacer layers introduces an additional leading parameter. In the first part of this report we have shown how, when burying highly strained wires, the surface morphology combined with the strongly inhomogeneous strain distribution favors partial demixing of the spacer layer. The calculated demixing matches the V-shape experimentally observed. Then, starting from this point, we have studied its consequences on the vertical organization when depositing a second wire layer. In practice, depending on design parameters, almost all configurations can be obtained (from perfect top-on-top, to perfect vertical anticorrelation, via all kinds of oblique correlation). It is interesting to note that the oblique correlation we obtain is basically different from that proposed by Holý *et al.* in Ref. 9. In Ref. 9 indeed, the oblique vertical alignment is attributed to the anisotropic behavior of the materials. For the systems we have studied here, the anisotropy is not strong enough to induce such an alignment [this has been demonstrated in Figs. 3(d)–3(f)]. Our oblique

correlation directly results from the shape of the partial spacer layer demixing. We have restricted our study to systems with a flat spacer layer surface. This is somewhat unrealistic in practice for the case of very thin spacer layers. It would be interesting to extend the study to rough spacer layers but this goes beyond the scope of this paper.

ACKNOWLEDGMENTS

The authors thank G. Hollinger for a constructive reading of the first draft of this manuscript, and Julien Brault and Michel Gendry for fruitful discussions of their experimental results.

-
- ¹Q. Xie, A. Madhukar, P. Chen, and N.P. Kobayashi, *Phys. Rev. Lett.* **75**, 2542 (1995).
- ²J. Tersoff, C. Teichert, and M.G. Lagally, *Phys. Rev. Lett.* **76**, 1675 (1996).
- ³Y.W. Zhang, S.J. Xu, and C.H. Chiu, *Appl. Phys. Lett.* **74**, 1809 (1999).
- ⁴G.S. Solomon, J.A. Trezza, A.F. Marshall, and J.S. Harris, *Phys. Rev. Lett.* **76**, 952 (1996); *J. Vac. Sci. Technol. B* **14**, 2208 (1996).
- ⁵C. Teichert, M.G. Lagally, L.J. Peticolas, J.C. Bean, and J. Tersoff, *Phys. Rev. B* **53**, 16 334 (1996).
- ⁶B. Legrand, J.P. Nys, B. Grandidier, D. Stiévenard, A. Lemaître, J.M. Gérard, and V. Thierry-Mieg, *Appl. Phys. Lett.* **74**, 2608 (1999).
- ⁷B. Lita, R.S. Goldman, J.D. Phillips, and P.K. Bhattacharya, *Appl. Phys. Lett.* **74**, 2824 (1999).
- ⁸W. Wu, J.R. Tucker, G.S. Solomon, and J.S. Harris, *Appl. Phys. Lett.* **71**, 1083 (1997).
- ⁹V. Holý, G. Springholz, M. Pinczolits, and G. Bauer, *Phys. Rev. Lett.* **83**, 356 (1999).
- ¹⁰G. Springholz, V. Holý, M. Pinczolits, and G. Bauer, *Science* **282**, 734 (1998).
- ¹¹V.A. Shchukin, D. Bimberg, V.G. Malyshekin, and N.N. Ledentsov, *Phys. Rev. B* **57**, 12 262 (1998).
- ¹²J. Brault, M. Gendry, O. Marty, M. Pitaval, J. Olivares, G. Grenet, and G. Hollinger, *Appl. Surf. Sci.* **162-163**, 584 (2000).
- ¹³M. Gendry, J. Brault, C. Monat, J. Kapsa, M.P. Besland, G. Grenet, O. Marty, M. Pitaval, and G. Hollinger (unpublished), and Julien Brault, thesis, Ecole centrale de Lyon (2000).
- ¹⁴C. Priester and G. Grenet, *Phys. Rev. B* **61**, 16 029 (2000).
- ¹⁵J.E. Oh, P.K. Bhattacharya, Y.C. Chen, O. Aina, and M. Mattingly, *J. Electron. Mater.* **19**, 435 (1990).
- ¹⁶C. Priester, *Phys. Rev. B* **63**, 153303 (2001).